Non-Destructive Resonant Frequency Measurement on MEMS Actuators

Norman F. Smith[1], Danelle M. Tanner[1], Scot E. Swanson[1], and Samuel L. Miller[2]

[1]Sandia National Laboratories, P.O. Box 5800, MS 1081, Albuquerque, NM 87185-1081
email: smithnf@sandia.gov http://www.micromachine.org
[2]MEMX, Inc. 5600 Wyoming Blvd. NE, Suite 20, Albuquerque, NM 87109

ABSTRACT

Resonant frequency measurements provide useful insight into the repeatability of MicroElectroMechanical Systems (MEMS) manufacturing processes. Several techniques are available for making this measurement. All of these techniques however, tend to be destructive to devices which experience sliding friction, since they require the device to be operated at resonance. A non-destructive technique will be presented which does not require the device to be continually driven at resonance. This technique was demonstrated on a variety of MEMS actuators.

INTRODUCTION

Parametric measurements are at the heart of microelectronics manufacturing. These measurements allow the manufacturing processes to be continually monitored and corrections to be made when necessary. Without these crucial measurements the mass production of microelectronics would soon be impossible. The growing MEMS industry is in need of similar parametric measurements that can provide the insight required to control these processes. This will provide the yields necessary for inexpensive mass production of microsystems devices.

Some of the required parametric measurements for MEMS, such as sheet resistance, contact resistance, and electrical line width are directly transferable from the microelectronics industry. MEMS devices also require measurements that have no microelectronics counterpart. Resonant frequency measurements are one of those with no microelectronics counterpart.

Several techniques are available to measure resonant frequency. These techniques range from manual and computer-controlled blur-envelope techniques [1] to sophisticated electronic measurements [2]. All of these techniques require that the device be operated at its resonant point for a considerable length of time. Operating these devices at resonance tends to be destructive to the device, especially those that have sliding frictional surfaces [3]. In this paper we present a technique that uses the viscous damping effect of the device. This technique still requires that the device be operated for a considerable amount of time. However, it does not require the device to be driven at its resonant point which can be destructive to a mechanical system. This technique is equivalent to plucking a taut string on a guitar and watching the oscillation die down over a period of time. This technique has been applied to several device types and compared with blur-envelope measurements.

BACKGROUND

Theory

A typical MEMS actuator consists of an energy transducer (i.e. electrostatic comb-drive, thermal expansion, etc.), an anchoring structure, which anchors the device to the substrate, and a structure that provides some type of restoring force to the system. An example of a very simple actuator is shown in Figure 1. This comb-drive system can be represented as a mass, spring, and damper system, as shown in Figure 2. When an energy pulse is applied, all mechanical systems of this form will exhibit some mode of damped oscillation occurring about its natural resonant frequency. This is known as viscously damped free vibration.

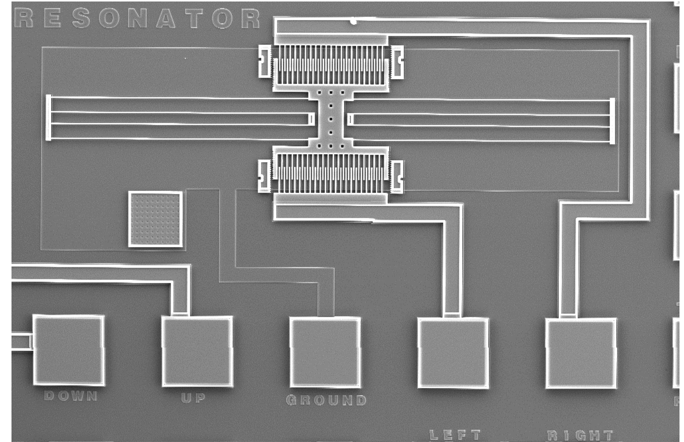

Figure 1. SEM image showing a simple comb-drive resonator.

From Newton's Law we know that $\Sigma F = ma$. From this we can easily derive the homogenous form of the differential equation

$$m\ddot{x} + kx + c\dot{x} = 0 \qquad (1)$$

where m is the mass of the actuator, k is the spring constant, and c is the proportionality constant of the damper. A traditional approach to solve this equation is to assume a solution of the form

$$x = e^{\lambda t} \qquad (2)$$

where λ is a constant. The general form of the solution to the differential equation is then

$$x = Ae^{\lambda_1 t} + Be^{\lambda_2 t}\,. \qquad (3)$$

After substitution and solving for the standard form, we obtain

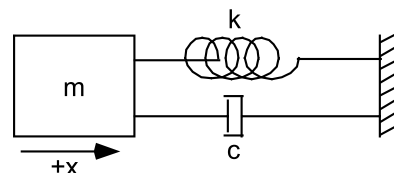

Figure 2. Schematic of a typical MEMS actuator.

$$\lambda^2 + \frac{c}{m}\lambda + \frac{k}{m} = 0 . \quad (4)$$

Now, we let $\frac{k}{m} = \omega_o^2$ and $\frac{c}{2m} = \delta$, the equation then becomes

$$\lambda^2 + 2\delta\lambda + \omega_o^2 = 0 \quad (5)$$

Solving for the roots of the equation, we obtain

$$\lambda = -\delta \pm \sqrt{\delta^2 - \omega_o^2} \quad (6)$$

Because we are solving for the case when the roots are imaginary (Under-damped case), we can substitute $-\omega^2 = \omega_o^2 - \delta^2$. After substitution of terms and solving for the constants in equation (3) our solution becomes

$$x(t) = x_o e^{-\delta t}\left[\cos(\omega t) + \frac{\delta}{t}\sin(\omega t)\right] . \quad (7)$$

An under-damped system will behave similar to the function shown in Figure 3a. One alternative case occurs when only a single real root can be determined. This results in a critically damped system whose behavior is shown Figure 3b.

In practice the displacement (x) is found by measuring the movement from a reference point on the actuator, and t is known from the time spacing at which the displacement measurements are taken. The terms in equation (7), resonant frequency component (ω), the damping term (δ), and the center-line displacement (X_o), can all be solved for by using a three parameter fit.

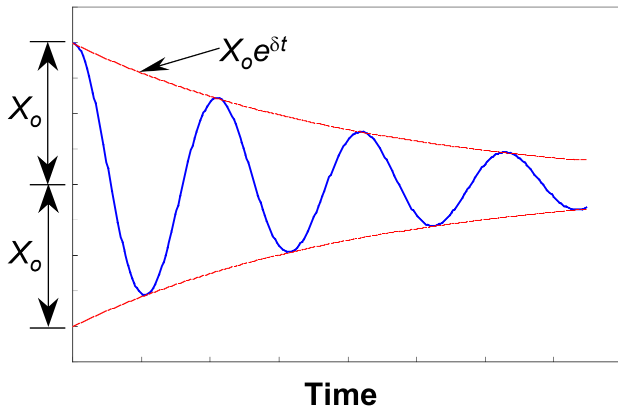

(a) Under damped system.

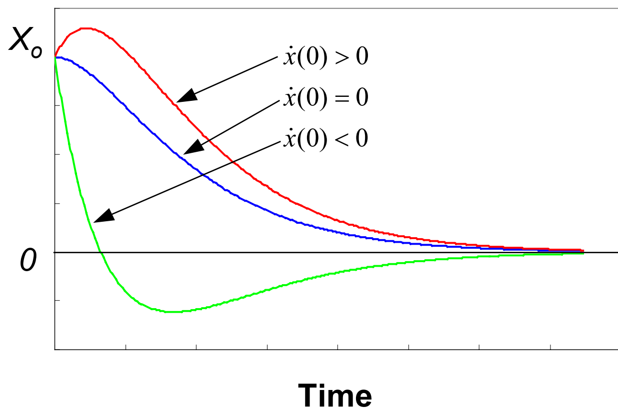

(b) Critically damped system.

Figure 3. Examples of viscous damped oscillations.

Data Collection System

In order to make the required displacement measurements, we need a method to measure the movement of the device accurately and repeatably in time. Two methods immediately come to mind. The first method would be to use a high-speed digital camera to capture the motion of the device in real time as the damped oscillation occurs. This method allows the entire set of data to be collected during a single actuation of the device. This method, however, is costly to assemble. An alternative method is to use stroboscopic illumination of the device. A stroboscopic system can be assembled relatively inexpensively. However, a disadvantage of such a system is that the device must be actuated many times to obtain a complete set of data. This is due to the fact that it may require multiple actuations of the device in order to collect a single image. For example, if the device is driven at 480Hz and it takes 1/30 of a second to capture a frame of video, the device will experience at least 16 actuations per image acquired. Others [4, 5] have constructed such stroboscopic illumination systems for MEMS devices and have had very good success with their overall operation.

The stroboscopic system used for the measurements of viscous damping described in this paper consists of a central computer that controls a strobe light source, waveform generator, video camera, and digital timer circuitry. A block diagram of the system is shown in Figure 4.

A waveform generator (not shown) is configured to output a synchronized pulse that acts as a timing signal. The timing signal coincides with the beginning of each waveform period. This synchronized pulse is then fed into the timer circuitry, which performs a divide-by-N function to step down the possibly multiple kilohertz actuation signal into a range acceptable for the strobe light. This divided signal is sent to a phase-delay circuit, which generates a time-delayed trigger. The time delay amount is determined by the interval at which the images are spaced. The trigger pulse is then routed to the strobe light and optionally to the video capture card. By adjusting the phase of the strobe light relative to the beginning of the actuation signal, a series of images as a function in time can be acquired. For the data presented in this paper, the image capture

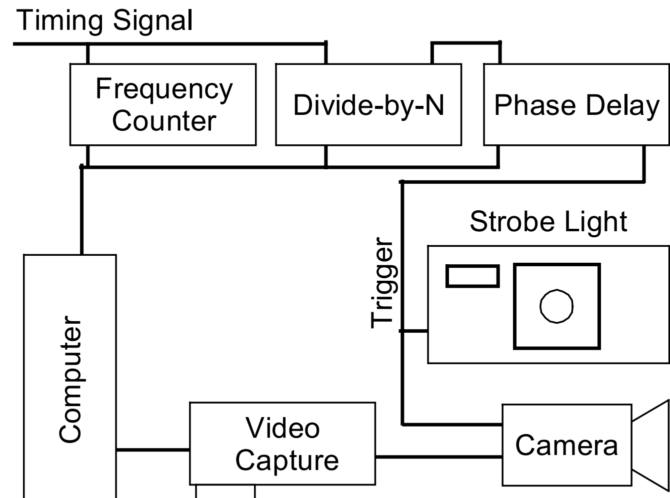

Figure 4. Block diagram of image capture system.

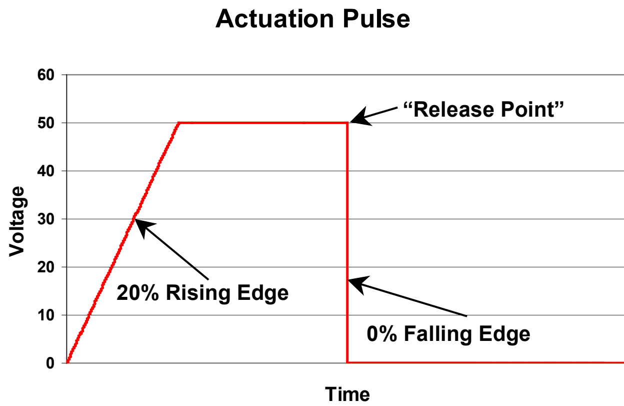

Figure 5. Graph of typical actuation waveform used to "pluck" device.

system was configured to start image acquisitions just prior to the actuation signal being removed from the device. The point at which this return occurs will be referred to as the "release point".

After the equally spaced image data are collected, displacement needs to be determined. From the images taken, a unique search target must be identified that can be used to determine the displacement of the actuator. Ideally this target should be relatively large and unique on the entire structure. A unique target would typically require that the actuator be redesigned or changed in some manner. Because design changes are usually not an option, an existing feature on the device can be used, provided it is never obscured and there are no others like it in the defined search region.

This displacement data along with the time information are used in a three-parameter model fit in order to determine the resonant frequency. The parameters are iterated until the sum of the errors is minimized. The resulting model fit yields the calculated resonant frequency and a damping coefficient.

EXPERIMENTAL APPROACH

This technique of measuring the viscous damping stroboscopically was applied to several types of MEMS devices. Actuation waveforms were chosen such that the initial actuation overshoot was minimized and that the device was allowed to stabilize before the voltage waveform drops, releasing the device from its actuated position. A typical actuation waveform is shown in Figure 5. This waveform has a rising edge of 20% of the period and a 0% falling edge. Image data were obtained on each of the devices and analyzed in a similar manner. Blur-envelope resonance measurements were taken on the same devices. A second operator performed the blur-envelope measurements to avoid measurement bias in the data.

Comb Resonators

Comb-resonators as shown in Figure 1 were measured in order to prove that this measurement concept was feasible. A total of eight devices were measured. The devices were driven with a waveform such as described in Figure 5. The waveform's amplitude was set to 55 V_{peak} with a frequency of 480 Hz. The design resonance point is several kilohertz. The actuation signal was chosen to ensure that the strobe was triggered often enough to provide an adequate amount of light for the video camera and to be at a multiple of the camera's shutter speed. Magnification was chosen to fill the available field of view. Using the smallest field of view possible allows smaller displacements to be observed. This small field of view also provides a greater range of displacement that allows a better fit to the measured data. Since these devices did not have any unique features on them, a repeated feature was chosen such that no other one like it would enter the search region. The search target used for measuring the displacements is shown in Figure 6.

A series of 250 images were taken on each resonator. Image collection began at 175° after the start of the waveform period. The phase-delayed trigger was then moved to capture the next image in the time sequence. The phase-delayed trigger was allowed to re-stabilize before the next image was taken. The strobe light required approximately 500 ms to reacquire this new trigger. Image collection continued up to 300° from the start of the waveform period. The images were processed using IMAQ Vision Builder [6] and the target information was imported into Excel for final model determination. Excel's solver engine was used with equation (7) to solve for the resonant frequency of the device. Model fit errors were calculated from the sum of the square of the difference between the measured value and the calculated value. The model fit error was then reduced to a change in resonant frequency. The change in frequency was determined by calculating two separate resonance curves separated by the model fit error. A typical plot of the image data and model fit is shown in Figure 7.

The blur-envelope measurements were made using a DC-offset sine wave with the amplitude adjusted to achieve the maximum displacement possible without the device hitting any of its mechanical stops. The resolution for this type of resonance measurement is typi-

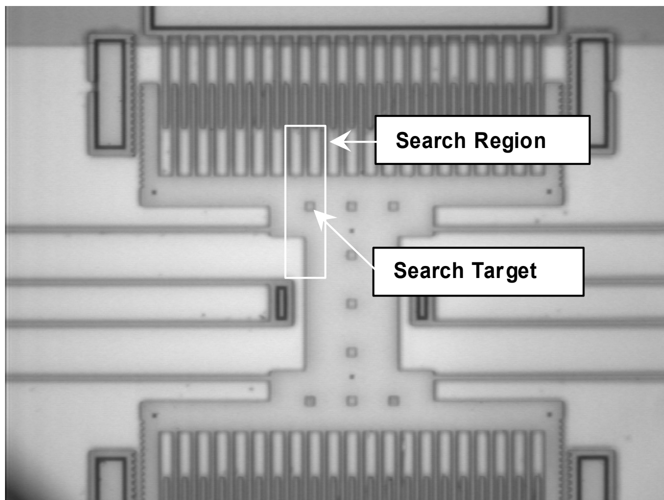

Figure 6. Resonator showing search target and region of interest.

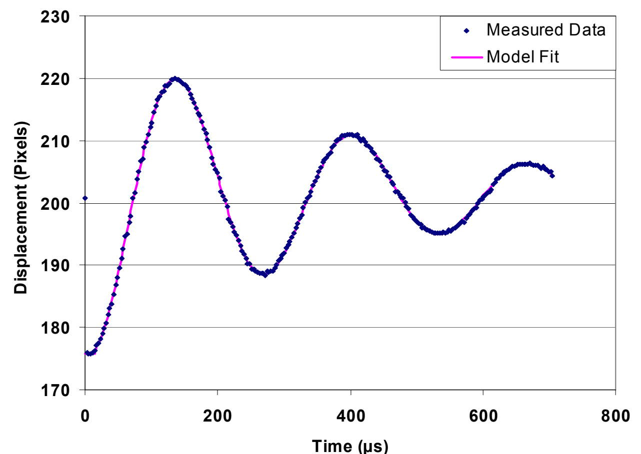

Figure 7. Model fit to measured displacement data.

cally ±100 Hz. This is very dependent on the operator and the field of view available.

The results comparing both types of measurements are presented in Table 1. The damped-oscillation method shows very good correlation to the blur-envelope technique. The model fit error is shown in units of displacement squared and can be large. However, a better indication the actual measurement error is to use the fitting error. The fitting error shows an overall accuracy of about one percent.

One of the resonators, as shown in Figure 8, does not damp out correctly at the end. This can cause the model fit to have a large error value. The damping anomaly may be due to a small particle rubbing against the moving shuttle area creating an additional damping action for small motions. A particle is suspected since other small particles appeared around this resonator. Even with this large fit error, we still obtain results that are well within the measurement error from the blur envelope technique.

Serial Number	Damped Oscillation (Hz)	Model Fit Error	Fitting Error (Hz)	Blur Envelope (Hz)
2303-1	4061	120.35	±42	4000
2303-2	4063	80.67	±36	4100
2303-3	4003	165.81	±33	4000
2304-1	4153	25.96	±21	4100
2304-2	4090	108.14	±53	4000
2304-3	4084	29.27	±29	4000
2312-1	3681	25.82	±22	3700
2312-3	3779	13.81	±17	3800

Table 1. Comparison of resonance measurement methods.

A repeatability study was then performed on an additional resonator. Nine separate measurements were performed on this resonator. The number of images acquired was varied after every three measurements. For each measurement, the device was removed from the test setup and then replaced. Adjustments were made to restore the position and focus in order to set up the part for the measurement. Data were acquired and analyzed using the same waveform and analysis method that was used with the individual resonators.

The resonator chosen for the repeatability studies had some of the largest error values when compared with the other resonators used for these experiments. The large fit errors may be due to the introduction of particles or other contamination since the resonators should be frictionless devices. A sample of the 75-point data is

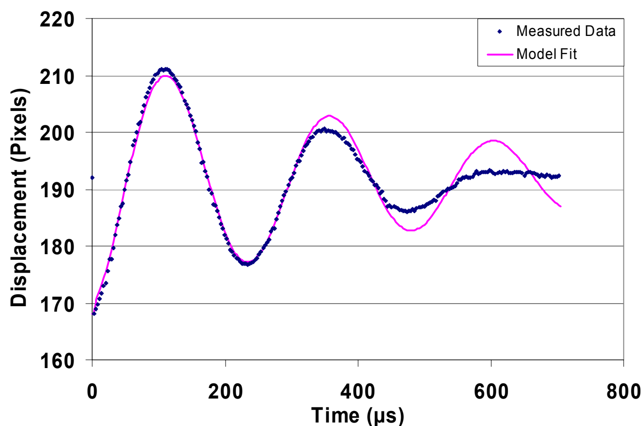

Figure 8. Effect of additional damping component on small amplitude motions.

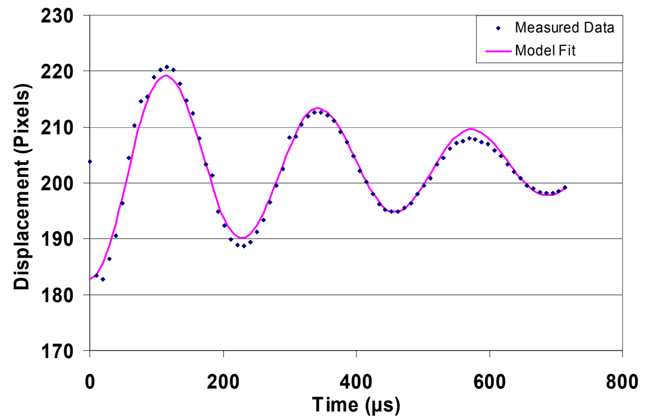

Figure 9. 75-point repeatability data shows non-periodic motion.

shown in Figure 9. The 75-point data shows that this device is not always periodic in its motion. This shows up as image points that are not equally spaced in time. The non-periodicity coupled with the sparse points during the initial oscillation period influences the model fit equation fairly heavily. Note that the model agreement is much better toward the end of the oscillation curve where the points are more evenly spaced.

Measurements were repeated on this part using both 125- and 250-points. The results are presented in Table 2. The 75-point data has a tendency to report higher resonance values than the 125- and 250 point measurements. The higher values may be due to an insufficient number of points early in the first period of oscillation. However, this measurement still falls within the measurement range expected from a blur-envelope measurement. The 125- and 250-point measurements show reasonable agreement. This indicates that measuring this type of resonator using only 125-points would be sufficient to yield accurate results. The device still shows its non-periodic motion in these images (Figure 10), but there are more evenly spaced points giving the model a better chance at calculating a good fit.

Points Taken	Run	Resonance (Hz)	Model Fit Error	Fitting Error (Hz)
75	1	4347	73.64	±72
75	2	4363	109.54	±87
75	3	4343	85.33	±78
125	1	4279	52.58	±48
125	2	4295	64.91	±52
125	3	4281	68.93	±53
250	1	4282	160.74	±58
250	2	4287	84.20	±42
250	3	4292	122.05	±51

Table 2. Repeatability for varied image points.

Sandia Microengine

The damped-oscillation measurement technique was then applied to a different type of device. The Sandia microengine was used to demonstrate that this technique can be used to determine a system resonance. The microengine has been used extensively for characterization and reliability studies [7, 8, 9] and its operation is fairly well understood. The Sandia microengine consists of orthogonal linear comb-drive actuators mechanically connected to a rotating gear as seen in Figure 11. By applying the proper drive voltages, the linear displacement of the comb drives is transformed into circular

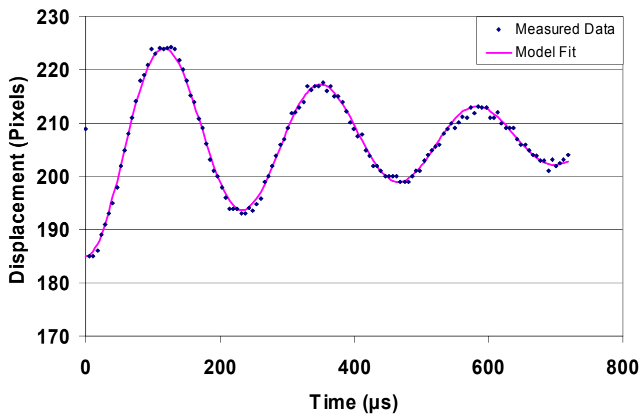

Figure 10. 125-point data still shows evidence of non-periodic motion.

motion. The X and Y linkage arms are connected to the gear via a pin joint. The gear rotates about a hub, which is anchored to the substrate. The Sandia microengine requires four phase-separated drive signals for normal operation. In order to perform a resonance measurement on the device only a single signal is required. The acutation signal was applied to the right comb drive and the remaining comb drives were grounded.

A set of three microengines was used to determine the applicability to a more complex actuator. All three of the actuators were located on the same die. A waveform pulse of 67.5 V_{peak} was applied to the right-left shuttle assembly on the microengine. A suitable target was found at the connection of the support springs to the shuttle assembly. Data was acquired on each microengine on the die. Since each microengine on the die is rotated 90 degrees from the previous, it was necessary to rotate the camera when measuring in order to measure the shuttle assembly on the same camera axis. After the image data had been successfully acquired blur-envelope measurements were taken. Results for the microengine experiment are shown in Table 3.

Two of the three microengines failed during fine-tuning of the blur image. These failures can be attributed to the fact that blur-envelope measurements are done at the device's resonant frequency and can require a considerable amount of time to narrow in on the resonant point. Operation at the resonance point has been shown to cause the device to degrade quickly [3]. The maximum displacement was noted to occur at approximately 1.5 kHz but further refinement

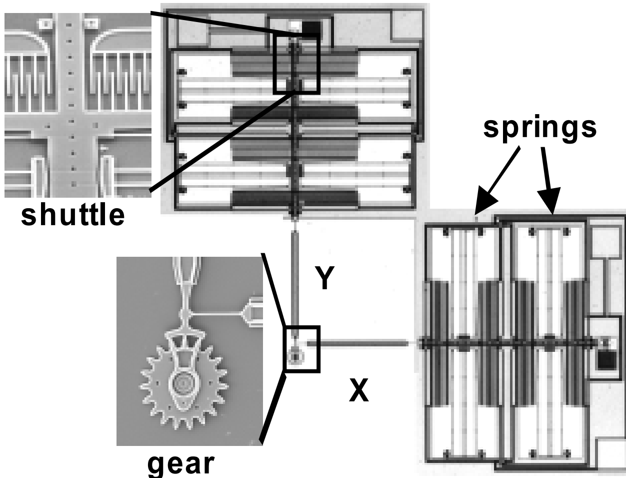

Figure 11. Sandia microengine with expanded views of the comb drive (top left) and the rotating gear (bottom left).

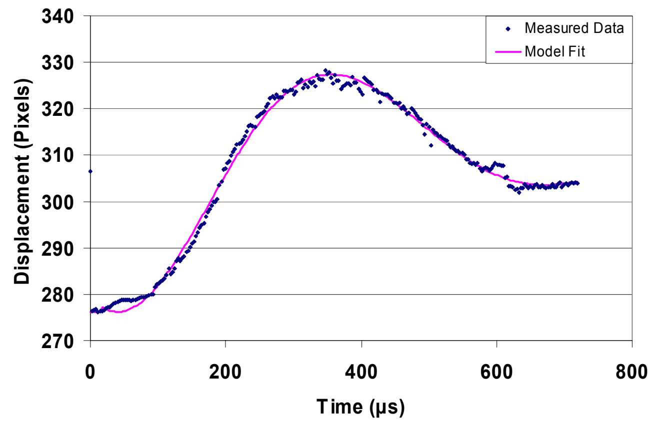

Figure 12. Microengine shows a different type of damped behavior.

was not possible. A successful blur measurement was made on the third microengine. The third engine's resonant point was determined to be 1.5-1.6 kHz. No noticeable change could be observed at these frequencies. The amplitude began to decay at 1.4 kHz and 1.7 kHz.

The errors encountered while determining a best-fit model are very large. After reducing this fit error to an actual change in frequency, the error is still inside of the range that was measured using the blur-envelope technique. In fact, the resonance point that was measured using the damped-oscillation method lies almost in the middle of where the successful blur-envelope result occurred. This shows that the damped-oscillation resonance measurement method can still extract very reasonable results even with large model fit errors. The behavior of the microengine's damped oscillation is more closely approximated by a critically damped system (Figure 3). This is due to the larger number of rubbing surfaces, which tend to enhance the damping effect. Figure 12 shows the results obtained when measuring microengine number two.

Engine	Damped Oscillation (Hz)	Model Fit Error	Fitting Error (Hz)	Blur Envelope (kHz)
1	1557	180.95	±33	~1.5
2	1587	400.47	±59	~1.5
3	1551	421.01	±57	1.5-1.6

Table 3. Microengine resonance values.

Electrically Damped Comb-Resonators

The comb-resonator and the microengine are bi-directional devices. These devices are designed to have the ability to move in either direction past their rest position. Many devices are designed to move in a single direction and may have mechanical stops preventing motion in other directions. The inability to move bi-directionally can cause the device to have inadequate room to recover correctly from the initial cycle of the damping curve. The device may actually impact its mechanical stops and prevent the continuation of the damped motion, preventing this technique from working. However, it may be possible to apply a constant bias to the device to move it sufficiently away from its mechanical stops to allow the damped motion to come to completion. Would applying a small steady state bias to a device effect the measurement? We return to our simple comb-resonator to find out.

In this experiment, we examined two separate resonators. Each resonator was measured with and without an external damping bias. The resonators without external damping were driven with a 45 V_{peak} pulse as shown in Figure 5. The resonators were then re-measured in the presence of an external displacement bias. The waveform was modified to allow a 15 VDC bias to be introduced. The amplitude of the drive pulse was reduced to 30 V_{peak} in order to prevent the shuttle from impacting its mechanical stops. The remaining test conditions were duplicated from the comb-resonator experiments.

Resonator	Normal Resonance (Hz)	Calculated Error (Hz)	Damped Resonance (Hz)	Calculated Error (Hz)
1	3669	±46	3670	±18
2	3776	±18	3784	±15

Table 4. Normal damping vs. externally applied damping field.

We notice that when the external damping field is applied, the resonant frequency is essentially the same, within the error of the technique. Resonator results from both cases are shown in Table 4. The external damping field does add one rather interesting aspect. It tends to tighten the model fit errors resulting in a better estimation of resonant frequency.

The addition of DC bias preloads the springs slightly. Because the fringing fields drive the resonator and the support springs are linear, this preload has the effect of displacing the springs from their normal rest position. This displacement should not affect the overall resonance unless the springs are extended past their linear regime. If large DC biases are applied, the springs can be displaced enough to become non-linear. This can cause the resonant frequency to shift and must be accounted for. A DC bias applied to a parallel plate actuator has a greater effect on resonant frequency. The bias can actually be used to tune the system to a known resonance point [10].

Torsional Ratchet Actuators (TRA)

The torsional ratchet actuator [11] is a surface micromachined actuator developed at Sandia as a lower voltage alternative to the microengine [12]. The TRA uses a rotational comb array for operation. A large circular frame holds the movable banks of comb arrays together. A SEM image of the fabricated TRA is shown in Figure 13.

Four cantilevered beams support the comb frame about its center and act as the frames spring return. These four beams are resistant to lateral motion but allow the frame to rotate. Three ratchet pawls and three anti-reverse pawls are located symmetrically around the outer ring. Four guides are used to constrain the motion and to maintain alignment of the ring.

In order to operate this device, a periodic voltage is applied between the stationary and moving combs. As the voltage increases, the movable comb frame rotates counter-clockwise about its springs. As the frame rotates, the ratchet pawls engage the outside ring causing it to rotate also. Once the combs have reached full travel the voltage waveform is decreased. The frame begins to move back to its rest position due to the restoring force on the springs. This movement drags the outside ring with it until the anti-reverse pawls engage. As the frame returns to its rest position the ratchet pawls engage the next tooth in the outer ring. This cycle is then repeated to create continuous motion.

In order to measure the resonance of the TRA is it necessary to disconnect the combs from the outer ring. This is necessary in order to avoid a change in mass during the damping cycle. The rotational

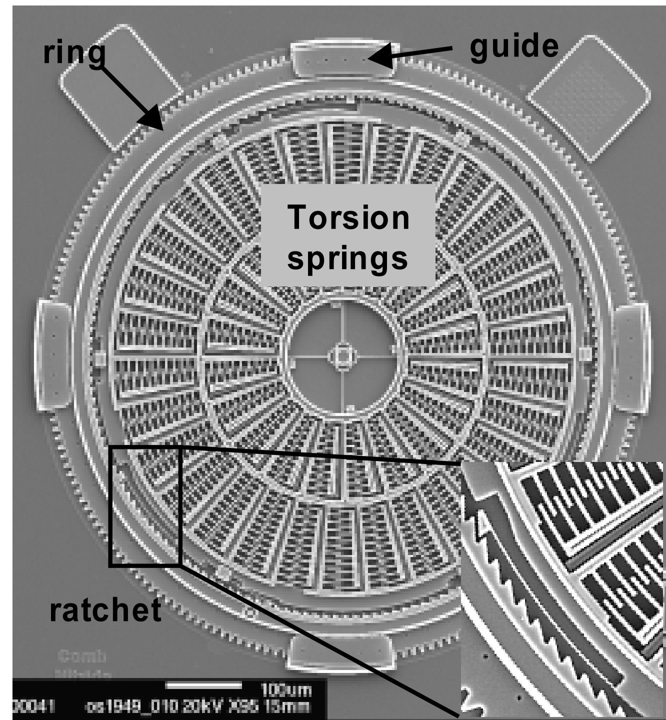

Figure 13. SEM image of a fabricated torsional ratchet actuator showing the ratchet and outer ring mechanisms. The inset shows an enlarged view of the ratchet.

mass changes since in the counter-clockwise direction both the comb frame and the outer ring are moving. During the clockwise return stroke only the comb frame moves. One TRA sample had the ratchet pawls removed. The second sample had the outer ring removed.

The TRA's combs are constrained to move only in the counter-clockwise direction. Mechanical stops in the comb structure prevent clockwise rotation of more than one micron. This limited travel requires that the combs be displaced slightly in order to use the viscous damping technique. This device was initially driven with a 7.5 VDC offset and an 18 V_{peak} drive signal. This configuration moved the combs several microns away from their stops. After the image data was analyzed it became very apparent that this amount of displacement was excessive. The data contains a fairly sharp discontinuity and flattened sections as shown in Figure 14. The discontinuity was caused from the impact of rotational combs into the mechanical stops. A new set of actuation conditions were determined in which

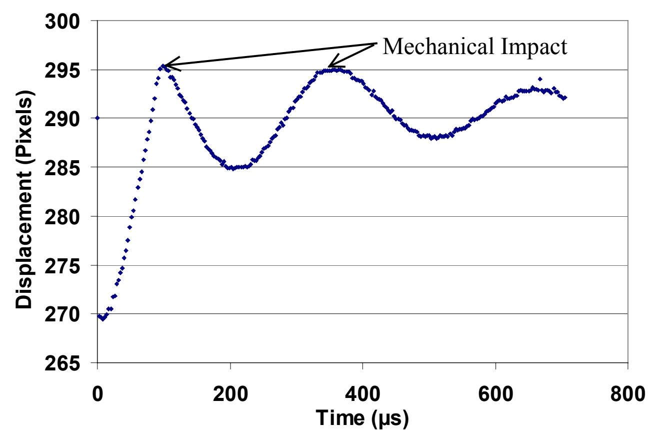

Figure 14. Mechanical travel limits prevent damping curve to occur properly. Flattened sections and discontinuities are due to mechanical stops on the TRA design.

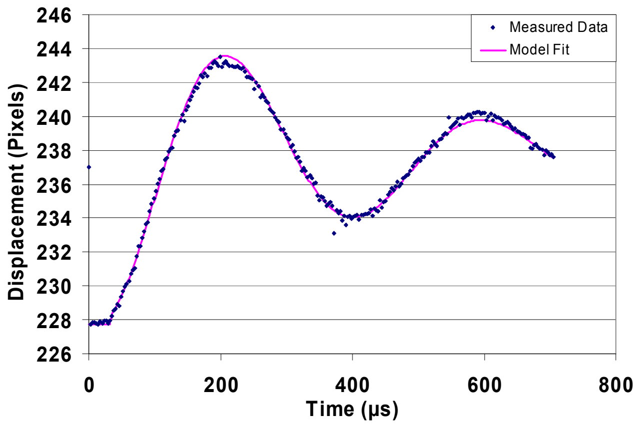

Figure 15. Viscous damping curve of TRA when not impacting mechanical travel limits.

the mechanical impact did not occur. The final conditions were a 7.5 VDC offset and a 7.5 V_{peak} drive signal. While these conditions produced an acceptable result, they were far from ideal. The displacement data was limited to about 16 pixels due to the fact that a higher power objective lens could not be used to view the device inside of its package. The resonant frequency result from one of the TRAs is shown in Figure 15.

The blur-envelope measurements for the TRAs shown in Table 5 exhibit a larger possible range for the resonant frequency. The TRA design incorporates non-linear springs for supports. These springs cause a hysteresis curve to appear in the blur-envelope measurement depending upon which direction the frequency is being swept. The large variation in the damped oscillation measurements can be attributed to sample preparation, since the removal of the ring gear can introduce damage to the movable comb structure.

TRA	Damped Oscillation (Hz)	Model Fit Error	Fitting Error (Hz)	Blur Envelope (kHz)
1	3288	25.83	±100	~2.5 – 3.5
2	2576	16.65	±48	~2.5 – 3.5

Table 5. Comparison of TRA measurements.

CONCLUSIONS

The technique of observing the viscous damping curve has been shown to provide acceptable values for resonant frequency when compared to the blur-envelope technique. This technique was successfully employed on several MEMS devices under varied condition. All of the viscous damped measurements lie within the error bound defined by the blur-envelope technique. The viscous damping technique has several advantages over the blur-envelope and other techniques that require the device to be operated at resonance. It doesn't require the device to be operated at resonance, which can significantly reduce is lifetime. This allows for larger collection of measurements to be performed instead of on a few sacrificial devices. Also, the viscous damping technique can be implemented inexpensively and can be configured to be fully automated.

A future enhancement would couple the viscous damping technique to an interferometer to determine resonant frequencies of devices that exhibit out-of-plane motions. This system could then be used to determine motions in three dimensions.

ACKNOWLEDGEMENTS

The authors would like to thank the personnel of the Microelectronics Development Laboratory at SNL for fabricating, releasing, and packaging the devices used for these experiments. We would also like to thank William Filter for discussions on conversion of model fitting error into an actual change in frequency.

Sandia is a multiprogram laboratory operated by Sandia Corporation, a Lockheed Martin Company, for the United States Department of Energy under Contract DE-AC04-940AL85000.

REFERENCES

[1] D. J. Burns and H. F. Helbig, "A System for Automatic Electrical and Optical Characterization of Microelectromechanical Devices," *Journal of Microelectromechanical Systems*, Vol. 8, No. 4, pp. 473-481, December 1999.

[2] T. C. Nguyen, "Electromechanical Characterization of Microresonators for Circuit Applications," *Final Report Masters Project*, The University of California at Berkeley, 1991.

[3] D. M. Tanner, W. M. Miller, W. P. Eaton, L.W. Irwin, K. A. Peterson, M. T. Dugger, D. C. Senft, N. F. Smith, P. Tangyunyong, and S. L. Miller, "The Effect of Frequency on the Lifetime of a Surface Micromachined Microengine Driving a Load," *1998 IEEE International Reliability Physics Symposium Proceedings*, March 30 - April 2, 1998, pp. 26-35.

[4] D. M. Freeman, Al J. Aranyosi, M. J. Gordon, S. S. Hong, "Multidimensional Motion Analysis of MEMS Using Computer Microvision," *Solid-State Sensor and Actuator Workshop*, Hilton Head Island, South Carolina, pp. 150-155, June 1998.

[5] G. F. LaVigne and S. L. Miller, "A Performance Analysis System for MEMS using Automated Imaging Methods," *Proceedings of IEEE International Test Conference*, Washington DC, pp. 442-447, October 1998.

[6] National Instruments, 11500 N. Mopac Expwy, Austin, TX 78759-3504.

[7] D. M. Tanner, N. F. Smith, D. J. Bowman. W. P. Eaton, and K. A Peterson, "First Reliability Test of a Surface Micromachined Microengine Using SHiMMeR," *Proceedings of 1997 Symposium on Micromachining and Microfabrication*, September 29, Austin, TX., Volume 3224, pp. 14-23, 1997.

[8] M. S. Rogers, J. J. Sniegowski, S. L. Miller, G. F. LaVigne, "Designing and Operating Electrostatically Driven Microengines," *Proceedings of the 44th International Instrumentation Symposium*, Reno, NV, May 3-7, 1998, pp. 56-65.

[9] D. M. Tanner, J. A. Walraven, L. W. Irwin, M. T. Dugger, N. F. Smith, W. M. Miller, and S. L. Miller, "The Effect of Humidity on the Reliability of a Surface Micromachined Microengine," *Proceedings of IEEE International Reliability Physics Symposium*, 1999, pp. 189-197.

[10] H. C. Nathanson, W. E. Newell, R. A. Wickstrom, and J. R. Davis, Jr., "The Resonant Gate Transistor," *IEEE Transactions on Electron Devices*, Vol. ED-14, No. 3, pp. 117-133, March 1967.

[11] S. M. Barnes, S. L. Miller, M. S. Rodgers, and F. Bitsie, "Torsional Ratcheting Actuating System," *International Conference on Modeling and Simulation of Microsystems*, San Diego, CA, March 2000, pp. 273-276.

[12] D. M. Tanner, S. M. Barnes, J. A. Walraven, N. F. Smith, F. Bitsie, S. Swanson, "Reliability of a MEMS Torsional Ratcheting Actuator," To be presented at the 2001 International Reliability Physics Symposium, Orlando, FL.